Effect of geometrical irregularities on propagation delay in axonal trees

Yair Manor,* Christof Koch,[‡] and Idan Segev*

*Department of Neurobiology, Institute of Life Sciences, Hebrew University, Jerusalem, 91904, Israel; and [‡]Computation and Neural System Program, California Institute of Technology, Pasadena, California 91225

ABSTRACT   Multiple successive geometrical inhomogeneities, such as extensive arborization and terminal varicosities, are usual characteristics of axons. Near such regions the velocity of the action potential (AP) changes. This study uses AXONTREE, a modeling tool developed in the companion paper for two purposes: (a) to gain insights into the consequence of these irregularities for the propagation delay along axons, and (b) to simulate the propagation of APs along a reconstructed axon from a cortical cell, taking into account information concerning the distribution of boutons (release sites) along such axons to estimate the distribution of arrival times of APs to the axons release sites. We used Hodgkin and Huxley (1952) like membrane properties at 20°C. Focusing on the propagation delay which results from geometrical changes along the axon (and not from the actual diameters or length of the axon), the main results are: (a) the propagation delay at a region of a single geometrical change (a step change in axon diameter or a branch point) is in the order of a few tenths of a millisecond. This delay critically depends on the kinetics and the density of the excitable channels; (b) as a general rule, the lag imposed on the AP propagation at a region with a geometrical ratio $GR > 1$ is larger than the lead obtained at a region with a reciprocal of that GR value; (c) when the electrotonic distance between two successive geometrical changes (X_{dis}) is small, the delay is not the sum of the individual delays at each geometrical change, when isolated. When both geometrical changes are with $GR > 1$ or both with $GR < 1$, this delay is supralinear (larger than the sum of individual delays). The two other combinations yield a sublinear delay; and (d) in a varicose axon, where the diameter changes frequently from thin to thick and back to thin, the propagation velocity may be slower than the velocity along a uniform axon with the thin diameter.

Finally, we computed propagation delays along a morphologically characterized axon from layer V of the somatosensory cortex of the cat (Fig. 5 b; Schwark and Jones. 1990. Brain Res. 78: 501-513). This axon projects mainly to area 4 but also sends collaterals to areas 3b and 3a. The model predicts that, for this axon, areas 3a, 3b, and the proximal part of area 4 are activated ~2 ms before the activation of the distal part of area 4.

INTRODUCTION

In the preceding publication (Manor et al., 1991), AXONTREE, a program for the simulation of action potentials (APs) propagating along axonal trees, was presented. In this study, AXONTREE was used to investigate the propagation delay expected in realistic axons, focusing on the effect of geometrical irregularities on this delay. Indeed, both experimental (e.g., Parnas, 1972; Grossman et al., 1979; Smith, 1983) and theoretical (e.g., Berkenblit et al., 1970; Goldstein and Rall, 1974; Khodorov and Timin, 1975; Parnas and Segev, 1979; Moore et al., 1983; Lüscher and Shiner, 1990a, b) studies show that geometrical inhomogeneities such as a change in axon diameter or a branch point with an impedance mismatch can lead to changes in the propagation velocity of the AP near the region of change. These studies, in particular that of Goldstein and Rall (1974), demonstrate that the behavior of the AP near the

branch point (as well as near an abrupt change in diameter) can be characterized by the geometrical ratio (GR), which is the ratio of the input impedance of the daughter branches to the input impedance of the parent trunk, as defined in Methods. When $GR < 1$, propagation is accelerated (relative to the uniform case where $GR = 1$) and the safety factor for propagation is increased. When $GR > 1$, propagation is delayed and may even completely fail in extreme cases. However, none of these studies investigated in detail the propagation delay expected at a region with a single geometrical change (with $GR \neq 1$) nor was the effect of the interaction among two or more branch points or varicosities studied. Because an AP propagating within an axonal tree with several thousand terminals must pass through on the order of 10–12 branch points, the total delay caused by these geometrical inhomogeneities per se could, in principle, be substantial.

In the following, we will first discuss propagation delays associated with single branch points or step changes in axon diameter. We will then discuss the

Address correspondence to Y. Manor, Department of Neurobiology, Institute of Life Sciences, Hebrew University, Jerusalem, 91904, ISRAEL.

interaction among more than one such inhomogeneity and compute the propagation delay expected along a morphologically reconstructed cortical axon. Finally, we discuss the implications of our results in terms of information transmission and processing along axons.

METHODS

All simulations were performed using AXONTREE. Details are given in the companion paper (Manor et al., 1991). In the first part of the study we explored the effect of an abrupt change in axon diameter (or a single branch point) per se on the propagation delay. In this part we were not interested in the delay produced along the uniform regions which, in an unmyelinated axon, is proportional to the space constant, λ (that is, proportional to the square root of the diameter). This holds provided that the specific membrane parameters (both passive and active) are uniform along the axon and one is not close to an end (Jack et al., 1975). Thus, when the distance, x, along the axons is normalized by units of λ, the velocity (the slope of AP peak-time vs. $X = x/\lambda$) is constant, independent of the axon diameter; it changes only near inhomogeneous regions. Therefore, to gain insights into the consequence of local geometrical changes per se on the propagation delay, the distance along the simulated axon was scaled in units of λ (Figs. 1–7). Local irregularities were characterized by the geometrical ratio, GR, defined as,

$$GR = \sum_i d_i^{3/2}/d_p^{3/2}, \qquad (1)$$

where d_i is the diameter of the ith daughter branch and d_p is the diameter of the parent branch. If the passive specific properties of the membrane (R_m, C_m) and the cytoplasm (R_i) are constant along the axon, and the daughter branches have the same electronic lengths and boundary conditions, then GR is the ratio of the sum of the input impedances of the daughter branches to that of the parent branch. If $GR = 1$, the input impedances are matched, implying that the safety factor for AP propagation does not change at the branch point. When $GR > 1$ the safety factor for AP propagation decreases, whereas when $GR < 1$ the safety factor increases (Goldstein and Rall, 1974). Note also that when GR is an integer > 1 (and the parent and daughter branches are electrically long), the GR factor corresponds to the number of daughter branches, each having a diameter identical to the parent diameter. For example, $GR = 2$ corresponds to the commonly occurring case where the two daughter branches have the same diameter as the parent axon.

For numerical stability, the spatial integration step, Δx, was $\lambda/10$ along uniform regions of the axon and $\lambda/100$ near regions of abrupt geometrical change (Parnas and Segev, 1979). The temporal integration step, Δt, was typically 10 μs. Unless otherwise stated, the membrane properties were those used by Hodgkin and Huxley (1952) and 20°C with specific cytoplasmic resistivity, R_i, of 100 Ωcm and specific membrane capacitance of 1 μF/cm^2. For these values and for an axon with a diameter of 1 μm, the space constant, λ, is $\sim$190 μm.

RESULTS

A single geometrical change

The change in AP shape and velocity near a region with a local geometrical change (with $GR = 8$) can be appre-

ciated in Fig. 1. In Fig. 1 A, a schematic drawing of an axon is shown. The parent branch bifurcates into two identical daughter branches, each having a diameter that is 2.52 times larger than the parent diameter (implying $GR = 8$). This axon is equivalent to a cable with an $8^{2/3}$ (=4)-fold increase in diameter (Goldstein and Rall, 1974). The AP recorded at three points along this structure is shown in Fig. 1 B (dashed curves). Point 1 is at a distance, x, of 2λ before the geometrical change; point 2 is at the branch point itself, whereas point 3 is at $x = 2\lambda$ after the branch point. For comparison, the continuous curves show the case where $GR = 1$, which is equivalent to a uniform axon. Indeed, in the latter case the shape of the AP is identical in all three recording points and its velocity (in units of λ) is constant. When
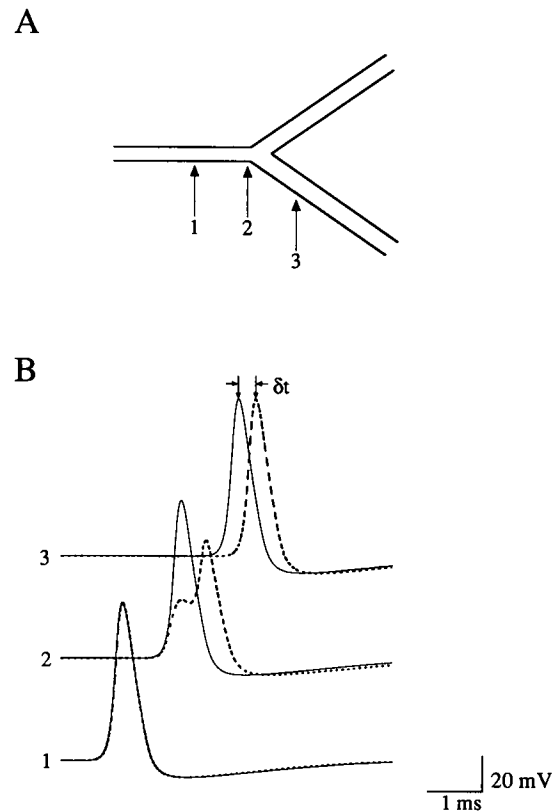

FIGURE 1 Induction of propagation delay along a bifurcating axon. In A, a scheme of a bifurcating axon is drawn. The GR associated with this branch point is 8. Arrows show recording locations: 1, is 2λ before the bifurcation; 2, is at the bifurcation; and 3, is 2λ after the bifurcation. In B, the shape of the AP at these three locations is shown (dashed curves). For comparison, the AP along a uniform axon at the same recording sites is superimposed (continuous lines). At location 1, the AP in the uniform axon and in the branched axon coincide. At location 2, a delay in the AP propagating into the branched axon appears and the shape of the AP changes. Distal to the branch point, at location 3, the AP resumes its uniform shape and appears with a delay, $\delta t = 0.397$ ms, relative to the uniform case.

$GR = 8$, however, both shape and velocity change along the axon (dashed curves in Fig. 1 B). Near the geometrical change (point 2) the AP undergoes a modulation in amplitude and shape, and it appears with a delay. After the change, at point 3, the AP recovers to its normal shape and appears with a delay, δt, of 0.397 ms relative to the uniform case.

The space-time curves in Fig. 2 A illustrate how the AP's peak time (t_{peak}) changes along an axon with a single branch point. The control is the uniform case where $GR = 1$; the other five curves represent t_{peak} versus X for five different GR values (see arrows). The vertical dashed line (at $X = 2.5$) shows the point of geometrical change. Along a uniform region of the axon the AP peak travels with a constant velocity of 2.843 λ/ms (slope of control curve in Fig. 2 A). When $GR \neq 1$, however, the input impedance in the vicinity of the geometrical change is altered, resulting in an increase (when $GR < 1$) or a decrease (when $GR > 1$) in the safety factor for AP propagation. The three upper curves in Fig. 2 A ($GR = 2$, 4, and 8) show the decrease in the propagation velocity before the geometrical change, whereas in the two lower curves ($GR = 0.5$ and 0.01) the velocity before the change increases. The situation reverses immediately after the change: the velocity increases when $GR > 1$, whereas it decreases when $GR < 1$. Then, a few tenths of λ further downstream, the velocity returns to its constant value. For example, observing the uppermost curve ($GR = 8$), a sharp jump in t_{peak} is seen before the change (dashed vertical line), indicating a decrease in AP velocity (to 0.18 λ/ms). Just after the change the slope is practically zero (infinite velocity), implying that this region fires simultaneously. At a larger distance to the right, the curve regains the same slope as the slope before the change (see comparable results in Berkenblit et al., 1970; Goldstein and Rall, 1974).

The propagation delay (δt) induced by a local geometrical change per se is calculated as the difference between t_{peak} at the right-most point on the control curve ($GR = 1$) and t_{peak} at the same point on the curve corresponding to a given GR value. For example, the difference between the peak-time at $X = 4$ in the uppermost curve and in the control curve is 0.397 ms. Namely, a single geometrical change with $GR = 8$ induces a propagation delay of 0.397 ms. Likewise, a severe narrowing (with $GR = 0.01$) in the axon induces a propagation lead (a "negative" delay) of less than 0.1 ms (lowermost curve in Fig. 2 A).

The behavior of the AP peak value (V_{peak}) along an axon with an abrupt geometrical change is depicted in Fig. 2 B. The corresponding GR values are marked on each curve. When $GR > 1$, the peak at the region of the geometrical change is decreased; this reduction is apparent already at a distance of 0.5 λ before the change. If
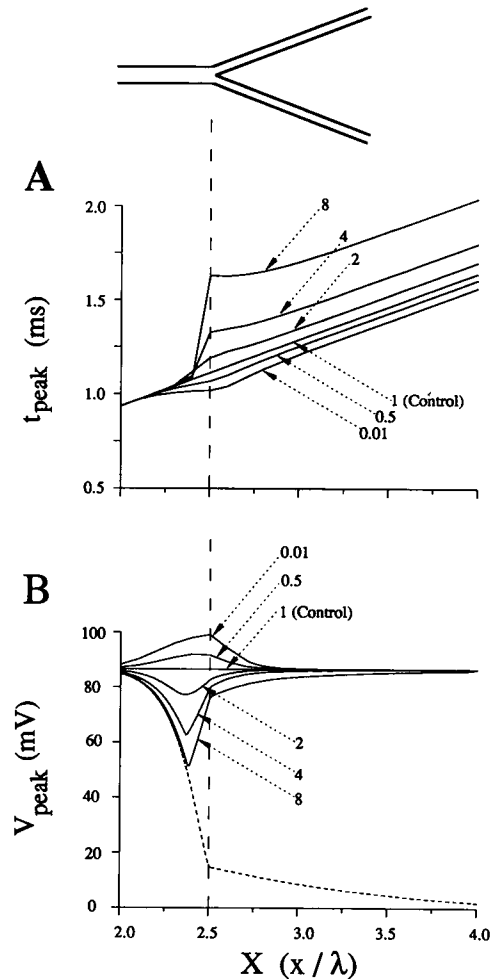

FIGURE 2 Action potential peak time and amplitude along an axon with a single geometrical change. In A, several space-time diagrams showing the AP peak time (t_{peak}) versus distance (in units of λ) are plotted for different values of GR (see arrows). The control curve corresponds to the case of an AP propagating along a uniform axon (equivalent to a bifurcating axon with $GR = 1$). When $GR > 1$, the AP peak is delayed with respect to the control. When $GR < 1$, the AP peak leads relative to the control. Note that, since distance is scaled in units of λ, all curves are parallel at $X = 4$. Hence, the delay (δt) induced by any particular GR per se can be calculated by simply subtracting the peak time on the control curve from the peak time on the curve with the corresponding value of GR, at a point where the slope of the curve has stabilized to a constant value. In B, the AP amplitude (V_{peak}) versus electrotonic distance for the corresponding GR values is plotted. In the case of $10.5 > GR > 1$, V_{peak} is reduced before the branch point but is restored to its original value after the branch point. The AP fails to propagate beyond the branch point for $GR > 10.5$, as exemplified by the dotted curve for the case of $GR = 11$. The vertical dashed line in both A and B (at $X = 2.5$) corresponds to the location of the branch point.

the AP propagates through the branch point (as is the case for $GR = 2, 4$, and 8), the minimal V_{peak} is obtained ~ 0.1 λ before the change. Thereafter, V_{peak} starts to grow back to the control amplitude (86.6 mV for the parameters chosen). In contrast, when $GR < 1$, V_{peak} starts to increase before the region of change (to almost 100 mV when $GR = 0.01$; *uppermost curve*); at $X = 0.5$ after the change the AP resumes its constant peak value. Note that when $GR = 11$ (*dashed curve*) the AP fails to propagate beyond the point of change.

The propagation delay, δt, calculated from curves similar to those shown in Fig. 2A is plotted in Fig. 3 as a function of GR. Here, the value of GR is plotted on a logarithmic scale, with the origin corresponding to the point $GR = 1$. In this way, any given GR value and its reciprocal value are equidistant from the origin. Two important points are noteworthy.

(*a*) For the parameter chosen, the lag due to a single geometrical change reaches 1 ms at $GR = 10$. Beyond that GR value propagation is blocked (e.g., *dashed curve* in Fig. 2B). On the other hand, the maximal lead obtained at a geometrical change with $GR < 1$ (relative narrowing) is less than 0.1. ms.

(*b*) The monotonic increase in the slope of the curve in Fig. 3 indicates that the lag produced as a result of any given $GR > 1$ is always larger than the lead produced at $1/GR$. Another outcome of this curve is that δt is a supralinear function of GR. For example, δt at $GR = 4$ is 0.157 ms, whereas at twice that GR value δt is 0.397 ms (δt increases by more than two-fold).

Clearly, δt will depend on the kinetics and density of the excitable channels. Indeed, in Fig. 4A the effect of temperature on δt in the case of a single geometrical
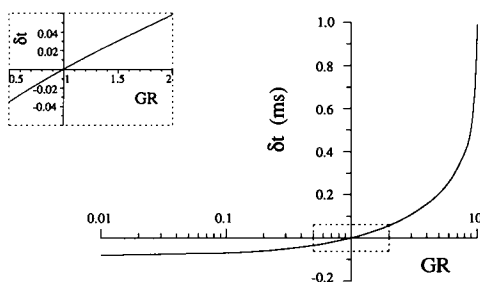
change with $GR = 2$ is examined. At low temperatures (low propagation velocity) δt is relatively large (0.191 ms at 0°C). This delay decreases to 0.053 ms (almost four-fold) when the temperature is increased to 25°C. Beyond this temperature, however, δt increases up to a point (of 33°C) where the AP is blocked at the geometrical change (*dashed line*). This result arises from opposing effects of temperature. Increasing the temperature reduces the duration and amplitude (i.e., the charge) of the AP (Huxley, 1959). This handicapped AP is more susceptible to propagation failure at regions of low safety factor (Westerfield et al., 1978), thus δt is expected to increase. On the other hand, when the temperature is increased, the threshold for initiation of an AP first reduces (the activation rate of sodium channels increases), whereas at high temperatures the

threshold rises (inactivation of sodium channels and activation of potassium channels increase). Hence, one should expect δt first to decrease and then increase with temperature.

The effect of channel density on δt for the case of $GR = 2$ is examined in Fig. 4 B. As expected, δt decreases as the density of the excitable channels that carry the inward current ($\bar{g}_{Na}$) increases. Note that the delay is very sensitive to the channel density for small values of $\bar{g}_{Na}$. When $\bar{g}_{Na}$ is too small (<55 mS/cm^2), the AP fails to propagate through the geometrical change (*horizontal dashed line*).

The results of this part of the study can be summarized as follows. At a region of a geometrical change the AP shape and velocity changes. When $GR > 1$, the AP peak is reduced and its velocity is decreased. As a result the AP is delayed at the region of the geometrical change and may completely fail when GR is above some critical value. Depending on the kinetics of the excitable channels, the delay due to a single geometrical change is on the order of a few tenths of a millisecond. When $GR < 1$, the AP near the region of change accelerates but the lead of the AP is small (i.e., less than 0.1 ms). In both cases the change in the AP shape and velocity is apparent already at a distance of ~ 0.5 λ before the geometrical change. The AP resumes its uniform shape and velocity several tenths of λ after the change.

Two successive geometrical changes

The results of the previous section can be used to gain insights into the behavior of the AP in a cable with two successive geometrical changes, one with GR_1 and the other with GR_2. It is clear that if the electrotonic distance between the two changes (X_{dis}) is sufficiently large, the behavior of the AP at each change is unaffected by the presence of the other change. Hence, the delay induced by the two geometrical changes is the sum of the two individual delays obtained at each change, when isolated. In the other extreme, when $X_{dis} = 0$, the delay (δt) is that expected in a single geometrical change whose corresponding GR value can be shown to be $GR_1 \cdot GR_2$ (this is also true for symmetrical trees which are equivalent to a single cable with two successive step changes in diameter; see footnote 1 below). The supralinearity in Fig. 3 also shows that, when $X_{dis} = 0$ (where $GR = GR_1 \cdot GR_2$) and both GR_1 and $GR_2 > 1$ (or both <1), the delay is larger than the linear sum of the individual delays. For such cases,

$$\delta t(GR_1 \cdot GR_2) > \delta t(GR_1) + \delta t(GR_2); \quad \begin{cases} GR_1, GR_2 > 1 \\ GR_1, GR_2 < 1. \end{cases} \quad (2)$$

For example, the delay in an isolated region with $GR = 3$, is 0.109 ms. When two such changes occur at

the same location, i.e., $X_{dis} = 0$, the delay is 0.516 ms, as expected from a single change with $GR = 9$, a highly nonlinear interaction. In an extreme case the proximity of two successive GRs > 1 may result in propagation failure which would not take place if the distance between the two changes were sufficiently large. e.g., when both GRs $= 4$ and X_{dis} is small (which, in the limit, corresponds to a single step with $GR = 16$) propagation fails (see Fig. 3).

Another relation which can be proved from Fig. 3 is that when one $GR > 1$ and the other $GR < 1$, and $X_{dis} = 0$, the delay is smaller than the delay expected from the linear sum of individual delays. Hence,

$$\delta t(GR_1 \cdot GR_2) < \delta t(GR_1) + \delta t(GR_1); \quad \begin{cases} GR_1 > 1, GR_2 < 1 \\ GR_1 < 1, GR_2 > 1. \end{cases}$$

$$(3)$$

For example, when $GR = 3$ (and δt is 0.109 ms in the isolated case) and $GR = \frac{1}{3}$ (and δt is -0.048 ms) then, when $X_{dis} = 0$ (and the corresponding GR is 1) the delay is 0 (whereas the linear sum is 0.061 ms).

What is the propagation delay expected when the distance, X_{dis}, between the two geometrical changes varies? The time-space diagram of Fig. 5 A demonstrates several such cases where both GR_1 and $GR_2 = 3$; Fig. 5 B treats the case where $GR_1 = 3$ and $GR_2 = \frac{1}{3}$. As in Fig. 2 A, the control curve shows the uniform case, where $GR_1 = GR_2 = 1$ (no delay). The other four curves in Fig. 5 A represent the case of an axon with two successive geometrical changes, in which $X_{dis} = 2$, 0.5, 0.1, and 0. In all cases, the first geometrical change is at $X = 2.5$ (*vertical dashed line*). As can be seen, when $X_{dis} \geq 0.5$, the delay in each change is unaffected by the presence of the other change. For example, the curves corresponding to $X_{dis} = 0.5$ and $X_{dis} = 2$ meet at their right-most side (at $X = 5$), and the delay contributed by both changes (0.218 ms) is exactly twice that contributed by an isolated change with $GR = 3$ (i.e., the two "jumps" in each of these curves are identical).

When $X_{dis} < 0.5$, however, the total delay is more than the linear sum of individual delays. In these cases, the interaction between the two successive changes results with an additional delay, δt^*. Hence, one can write:

$$\delta t(GR_1, GR_2, X_{dis}) = \delta t(GR_1) + \delta t(GR_2) + \delta t^*, \quad (4)$$

where $\delta t(GR_1, GR_2, X_{dis})$ is the delay contributed by two changes, the first with GR_1 and the second with GR_2, when separated by X_{dis}. This additional delay, δt^*, is a consequence of the impedance load imposed by the presence of a second geometrical change on the AP when propagating through the first geometrical change.
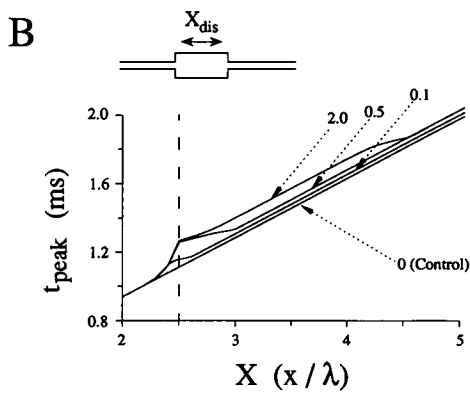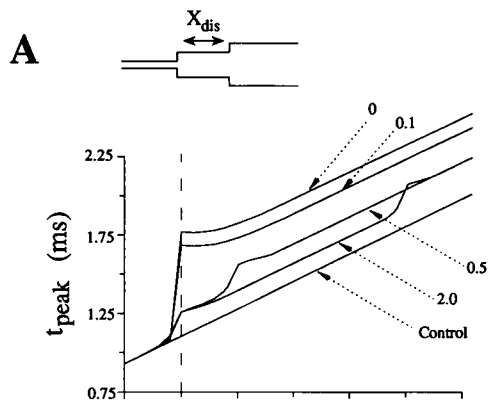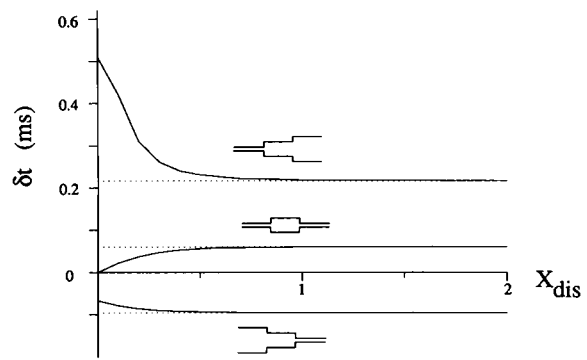
A

B

FIGURE 6   Effect of the electrotonic distance between two successive geometrical changes on the propagation delay. An axon with two successive geometrical changes, the first with GR_1 and the second with GR_2, is simulated. The total propagation delay, δt, was calculated as a function of the electrotonic distance between the changes (X_{dis}). The top curve and the inset correspond to $GR_1 = GR_2 = 3$, the middle curve to $GR_1 = 3$ and $GR_2 = \frac{1}{3}$, whereas the bottom curve plots δt for $GR_1 = GR_2 = \frac{1}{3}$. The middle curve is very similar to the case $GR_1 = \frac{1}{3}$ and $GR_2 = 3$ (not shown). In all cases, the total delay is the sum of the individual delays at each geometrical change, when X_{dis} is sufficiently large (> 1). For smaller X_{dis} values, the delay at the first change is affected by the presence of the second change, resulting in a larger lag (*top curve*), smaller lead (*bottom curve*) or a smaller lag (*middle curve*), as compared with the linear case (denoted by the corresponding *dotted horizontal lines*).

FIGURE 5   Space-time diagrams for an axon with two successive geometrical changes. In A, several space-time diagrams show the AP peak time (t_{peak}) along a 7λ long axon (first 2λ and last 2λ are not shown) with two successive geometrical changes, both with $GR_1 = GR_2 = 3$ (see the schematic at the top). The electrotonic distance between the two geometrical changes, X_{dis} (*arrows*), is varied among the curves. The lowest curve, marked control, corresponds to a uniform axon. Note that for $X_{dis} = 0$, a single geometrical change with $GR = 9$ occurs at the branch point. In B, $GR_1 = 3$ and $GR_2 = \frac{1}{3}$. Again, the space-time curves are for different values of X_{dis}. This situation corresponds to a uniform axon bearing a single, X_{dis} long, varicosity. The curve corresponding to $X_{dis} = 0$ is identical to the uniform (control) case. Vertical dashed lines in both A and B (at $X = 2.5$) indicate the point where the first geometrical change occurs.

Clearly, as seen in Fig. 5 A, this addition is maximal when $X_{dis} = 0$.

It is important to emphasize that the additional delay, δt^*, may be larger than the sum of individual delays obtained at each of the corresponding geometrical changes, when isolated. This is the case for $X_{dis} = 0$ in Fig. 5 A, where $\delta t^* = 0.298$ ms, whereas the sum of individual delays (when isolated) is 0.218 ms. This point will be further demonstrated in Fig. 6.

Another combination of two successive geometrical changes is demonstrated in Fig. 5 B. Here, $GR_1 = 3$ and

$GR_2 = \frac{1}{3}$. Again, the control curve is for a uniform axon. As found in Fig. 5 A, when $X_{dis} \geq 0.5$, the total delay (δt) is the linear sum of individual delays (i.e., $\delta t^* = 0$). Indeed, in these two cases the 0.109 ms delay induced by the first change (widening) sums linearly with the 0.048 ms lead (a negative delay) induced by the second change, to give at $X = 5$ a total delay of 0.061 ms. When $X_{dis} = 0.1$, however, the delay is smaller than the linear sum, implying that $\delta t^* < 0$. Note, that since $GR_2 = 1/GR_1$, $X_{dis} = 0$ corresponds to the uniform (control) case. The important point to note is that at $X = 5$ all curves lie above the control curve, implying that the lead due to the narrowing (where $GR = \frac{1}{3}$) is smaller than the lag at the widening (where $GR = 3$).

In Fig. 6, δt, the total lag (or lead) contributed by two successive geometrical changes, is calculated as a function of X_{dis}. In the top curve, $GR_1 = GR_2 = 3$ (see *inset*). As discussed above, when X_{dis} is large, the individual delays sum linearly (dashed horizontal line at $\delta t = 0.22$ ms). For smaller values of X_{dis}, the curve lies above the dashed line, implying that $\delta t^* > 0$. The middle curve depicts the case where $GR_1 = 3$ and $GR_2 = \frac{1}{3}$; again the dashed line is for the linear sum of individual delays. As mentioned in the context of Fig. 5 B, δt (the total delay) for this case is always positive, whereas δt^* (the additional delay due to interaction) is negative (curve lies

below the dashed line). It is noteworthy that the curve corresponding to the reverse case, where $GR_1 = \frac{1}{3}$ and $GR_2 = 3$, is essentially identical to this curve (not shown). Finally, when both $GR_1 = GR_2 = \frac{1}{3}$, the total delay is always negative (lead) whereas $\delta t^* > 0$ (curve lies above the dashed line).

Figs. 5 and 6 treat the case of single cables with two successive step changes in diameter. These cables are electrically equivalent to symmetrical trees with a second order branching. To complete the analysis of this section, the nonsymmetrical case (not equivalent to a single cable) should be examined. The important features of such a case were extracted by simulating a particular example schematically shown by the insets of Fig. 7. Here, a parent axon bifurcates with $GR_1 = 1$, giving rise to two daughter branches with identical diameters. At a distance X_{dis} from this bifurcation, a step change (or an equivalent bifurcation) with $GR_2 = 3$ occurs in only one of the daughters (lower branch in inset), whereas the sibling daughter branch continues uniformly. Because $GR_1 = 1$, the primary bifurcation is not expected to perturb the propagation speed (when measured in units of λ). Clearly, this is true when X_{dis} is large. What happens to the propagation through this branch point when X_{dis} is small?

Fig. 7A depicts the AP peak time as a function of electrical distance along the parent branch and the daughter with the geometrical change (continuous line in inset). In addition to the control curve (where $GR_2 = 1$), three cases are shown ($X_{dis} = 0.5, 0.1,$ and 0). The primary bifurcation is always at $X = 2$ (dashed vertical line). As expected, the slope of all curves remains constant until the AP is electrically adjacent to the region of the secondary geometrical change. Indeed, as X_{dis} increases, the "jump" in t_{peak} moves further to the right. The delay, however, is not identical in the three cases demonstrated; it increases as X_{dis} increases. This implies that, as the two changes become electrically close, the delaying effect of the secondary geometrical change, and thus δt, is reduced. The reason for it can be best explained when analyzing the extreme case where $X_{dis} = 0$. A simple calculation shows that this case is equivalent to an axon consisting of a single geometrical change with a new geometrical ratio, $GR_1^* = (GR_2 + 1)/2 = 2.$[1]

[1] In the general case, the parent branch (having a diameter of d_1) bifurcates into two daughter branches (with diameters d_2 and d_3). Each daughter then bifurcates, one with GR_2 and the other with GR_3, respectively. The limiting case when $X_{dis} = 0$ for both daughter branches, is equivalent to a single change with $GR_1^* = GR_2 \cdot d_2^{3/2}/d_1^{3/2} + GR_3 \cdot d_3^{3/2}/d_1^{3/2}$. When $d_2 = d_3$, $GR_1^* = (GR_2 + GR_3) \cdot GR_1/2$. When $GR_1 = GR_3 = 1$, and $X_{dis} = 0$, this case collapses to the case examined in Fig. 7.
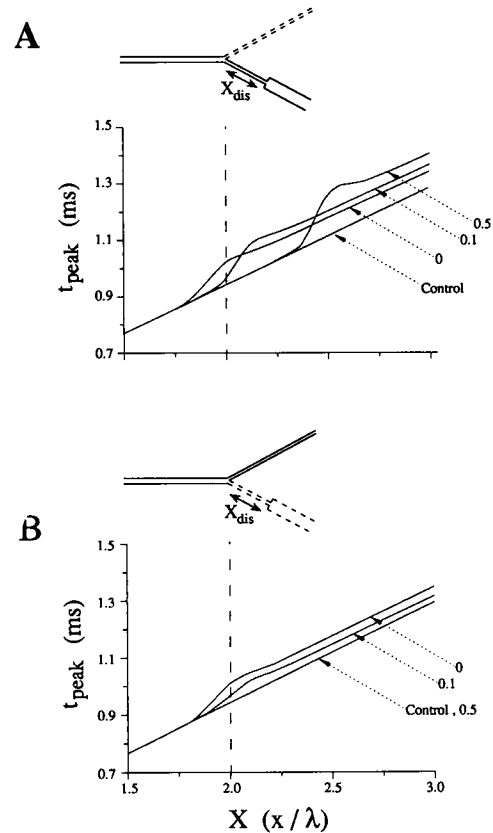

FIGURE 7 Space-time diagrams for a nonsymmetrically bifurcating axon. The parent trunk bifurcates (with $GR_1 = 1$), giving rise to two daughter branches. One daughter branch continues uniformly (top branch in both schematics), whereas along the lower branch a single geometrical change (with $GR_2 = 3$) occurs. The initial diameter of both daughter branches is identical. The branch point occurs at $X = 2$ (dashed vertical lines). In A, the AP peak time along the parent branch and the daughter branch with the geometrical change (continuous lines in schematic) is plotted for $X_{dis} = 0, 0.1$ and 0.5 (see arrows). The control curve is for the case where $GR_2 = 1$ (equivalent to a uniform axon). In B, the AP peak along the parent axon and the uniform daughter branch is plotted for the same X_{dis} values as in A. Note that the control curve (uniform axon) and the case for $X_{dis} = 0.5$ are indistinguishable.

Hence, the geometrical change ($GR_2 = 3$) that perturbs the propagation when X_{dis} is large, is reduced to a smaller change ($GR_1^* = 2$) when $X_{dis} = 0$. Note that for large values of X_{dis}, the delay due to the second geometrical change is identical to the delay in an isolated branch point with GR_2.

An interesting question is how propagation into the other (uniform) daughter branch is affected by the presence of a geometrical change in the sibling (nonuniform) branch. Fig. 7B shows that the propagation along this branch is delayed as a consequence of the change in the sibling branch but that, for the chosen GR_2 value of

3, this delay is apparent only when X_{dis} is small (0 and 0.1). When the secondary change at the sibling branch is 0.5 λ (or more) distal to the branch point, propagation along the other (uniform) daughter branch is not perturbed.

Frequent varicosities along the axon

A typical feature of axons in both vertebrates and invertebrates is the presence of multiple, closely spaced, varicosities or boutons. Electron microscopic (EM) studies have shown that these boutons are the main release sites of the neuron, and are typically associated with synaptic vesicles (McGuire et al., 1984; Schüz and Münster, 1985; Kisvarday et al., 1987). Careful measurements of bouton distribution in reconstructed axons in primate striate cortex (Florence and Casagrande, 1987), in cat striate cortex (Kisvarday et al., 1987), in the pontomedullary junction of the cat (Ohgaki et al., 1987), in the mouse neocortex (Hellwig B., A. Schüz, and A. Aertsen. Density and distribution of presynaptic boutons on Golgi-stained axons in the cortex of the mouse. Manuscript in preparation), and in other preparations show that, in these axons, the average distance between successive boutons is 4–8 μm. The diameter of the bouton may be two to five times larger than the interbouton diameter; the length of the bouton is typically 0.5–2 μm (McGuire et al., 1984; Schüz and Münster, 1985; Florence and Casagrande, 1987; Ohgaki et al., 1987; Peters, 1987; Rockland, 1989). The portion of the axon bearing varicosities is typically devoid of myelin (Fyffe and Light, 1984). The number of boutons within a single cortical axon can range between several hundreds (Rockland, 1989) to few thousands (Hellwig et al., manuscript in preparation). What is the consequence of such a frequent change in diameter for the propagation of APs along the axon?

Fig. 8A plots the AP peak-time (t_{peak}) versus anatomical distance along an unbranched, varicose, axon. The control is the case of a 600 μm long uniform axon having a diameter of 0.4 μm. In case a, the axon starts with an initial 100 μm uniform (0.4 μm) diameter; the next 500 μm is a varicose region, each varicosity (bouton) is modeled as a cylinder (a compartment) with a diameter and a length of 1.6 μm. The diameter of the axon between boutons is 0.4 μm and the interbouton distance is 4 μm (see inset). In case b, a single step increase in diameter (from 0.4 to 1.6 μm) occurs at x = 100 μm.

One should remember that, in contrast to previous figures, in Fig. 8A the abscissa is in anatomical units (μm). Thus, the slope of each of the curves is the reciprocal of the velocity, given in units of mm/ms. In a 0.4 μm uniform axon (control) the velocity is 0.347
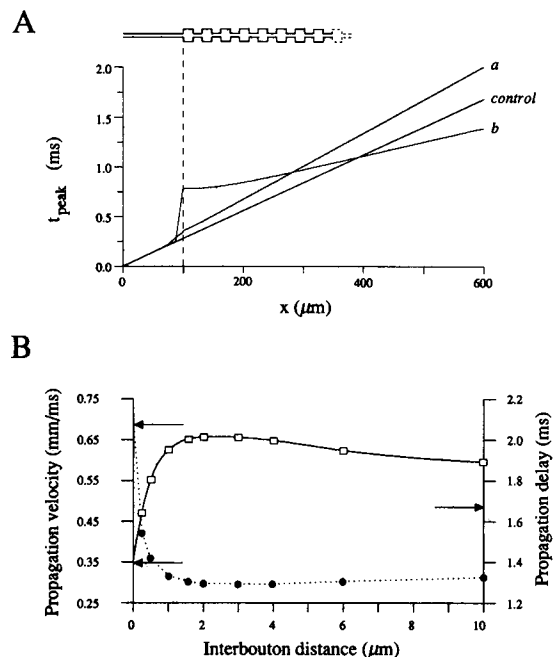

FIGURE 8   The propagation of an action potential along an axon with multiple varicosities. In A, three space-time diagrams are plotted. Here, the abscissa is given in anatomical units. The control case is for a 0.4 μm diameter, 600 μm long uniform axon. In curves a and b, the axonal varicosities start at x = 100 μm (dashed vertical line, see inset). Each varicosity is a 1.6 μm long, 1.6 μm wide cylinder. The interbouton diameter is 0.4 μm. In a, the interbouton distance is 4 μm, whereas in b it is 0 μm (the latter case is equivalent to an axon with a single step change in diameter, from 0.4 μm to 1.6 μm at x = 100 μm). Note that the inset is not drawn to scale: the frequency of the varicosities in curve a is much higher than pictured. In B, the effect of the interbouton distance on propagation velocity (left ordinate and filled circles) and propagation delay (right ordinate and empty squares) is shown. The bouton dimensions and the interbouton diameters are as in A. Top and bottom arrows in the left ordinate indicate the velocity in an axon with a uniform diameter of 1.6 μm (corresponding to the diameter of the boutons) and 0.4 μm (corresponding to the diameter of the axon between boutons). The arrow on the right ordinate indicates the propagation delay induced by a 600 μm long, 0.4 μm thick uniform axon.

mm/ms. This is comparable to estimations of propagation velocity in axonal collaterals in unmyelinated CNS neurons with similar diameters (Waxman and Bennett, 1972; Stone and Fukuda, 1974; Hsiao et al., 1984; Martin, 1984). In case b, the abrupt (four times) increase in diameter produces a marked delay at the geometrical change (dashed vertical line). After recovery, the AP reaches a constant velocity of 0.694 mm/ms, exactly twice the velocity of the control case. These two cases should be compared with case a (the varicose axon). Near the region where the varicosities start (vertical dashed line) a small delay in t_{peak} is obtained. Although
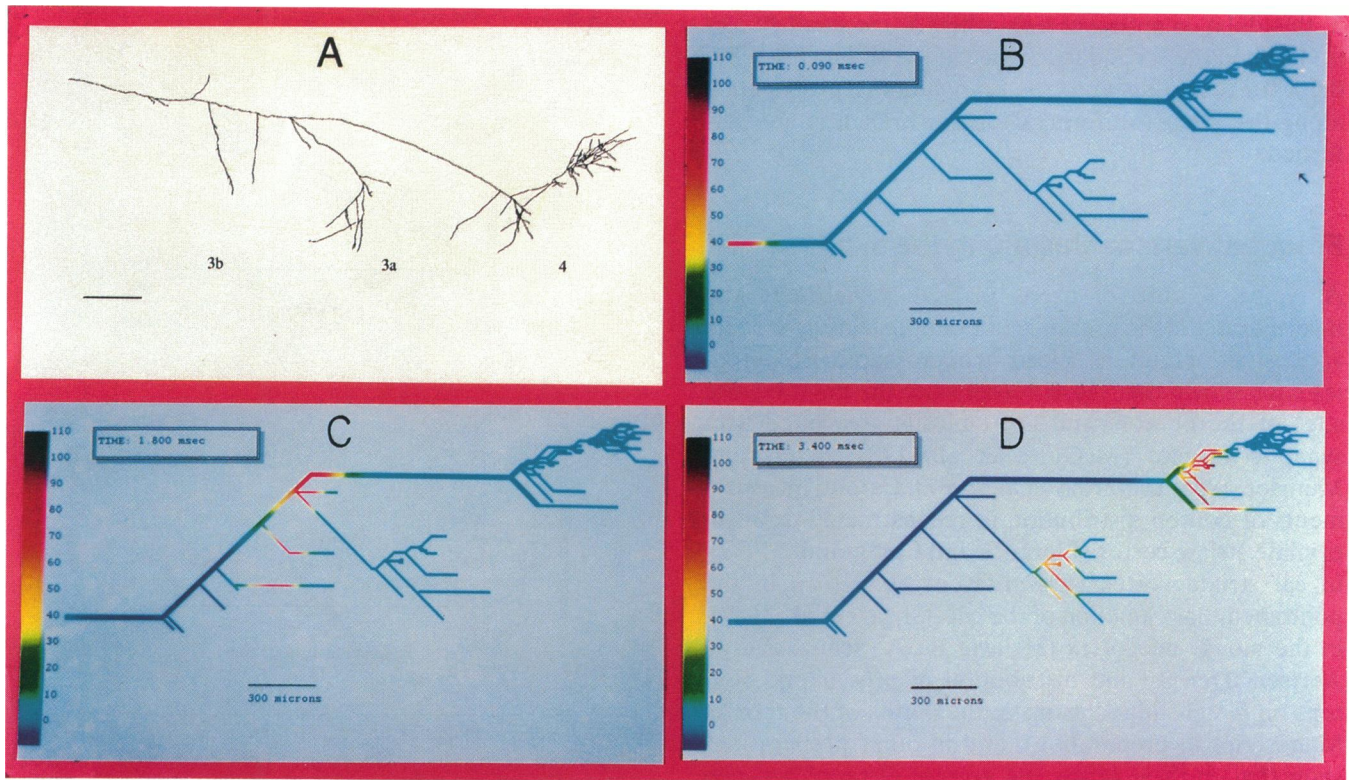
FIGURE 9   An action potential propagating along a morphologically characterized cortical axon. In A, a HRP labeled axon from the somatosensory cortex of the cat is shown (adapted from Schwark and Jones, 1989, Fig. 5 B). The calibration bar corresponds to 300 μm. B–D illustrate the distribution of voltage coded in colors (color scales given in mV relative to resting potential) along the simulated axon at three different times. The diameter of the main axonal process, first-order collaterals and higher order collaterals were assumed to be 2.5 μm, 1 μm, and 0.4 μm, respectively. Because most of the axon is confined to grey matter, we assumed it to be unmyelinated. Branches with a diameter of 0.4 μm were studded with boutons every 4 μm (a total of 977 boutons). Each bouton was modeled as a 1.6 μm × 1.6 μm cylinder. The axon was modeled with 2366 compartments using AXONTREE.

the diameter changes at this point are identical in both cases *a* and *b*, the presence of nearby successive bottle-necks (narrowings) in case *a* significantly reduces this initial delay, as compared with the delay in case *b*. Immediatly after entering the varicose region the slope of the curve becomes essentially constant, corresponding to a velocity of 0.29 mm/ms.[2]

The interesting finding is that, for the parameters chosen, the velocity along the varicose region is even

slower than the velocity in a uniform axon with 0.4 μm (interbouton) diameter (compare slope of curve *a* with the slope of the control curve). This is surprising because one intuitively expects the velocity to be between that in a 1.6 μm uniform axon (bouton diameter) and a 0.4 μm uniform axon (interbouton diameter). The reason for this result is that the lag, induced locally at each passage from the thin axon to the thick varicosity, is larger than the lead obtained at the passage from the varicosity to the thin axon (see Figs. 3, 5, and 6). The net delay at each varicosity accumulates, slowing down the propagation velocity even below that in a 0.4 μm uniform axon. An alternative explanation for the slowing down in Fig. 8 A curve *a* is that the AP propagating through a varicose axon "sees" local increases in membrane capacitance with a negligible decrease in intracellular resistivity. This explanation holds provided that the boutons are not too closely spaced. Indeed, when the interbouton

---

[2]We have also examined the more realistic case where the bouton diameter changes smoothly (rather than abruptly). Now the bouton diameter increases from 0.4 to 1.6 μm and decreases back to 0.4 μm in a sinusoidal fashion (each bouton was represented by 20 compartments). Only a small difference between this case and the case where the bouton was modeled by a step change in diameter was found. For example, the propagation velocity in case *a* of Fig. 8 A was 0.29 mm/ms for the cylindrical boutons, compared with 0.319 mm/ms for the sinusoidal boutons.

distance is very small, the intracellular resistivity is dominated by the bouton diameter, and the velocity is expected to increase (see Fig. 8 B, two *leftmost filled circles*).

How would changes in the interbouton distance affect the propagation velocity at the varicose region? This question is examined in Fig. 8 B. Here, the dimensions of each bouton are as in Fig. 8 A (case a) whereas the interbouton distance ranges from 0–10 μm. Top and bottom arrows in the left ordinate indicate the velocity in an axon with a uniform diameter of 1.6 μm (the bouton diameter) and 0.4 μm (the axon diameter), respectively. The filled circles indicate the propagation velocity along a varicose axon as a function of interbouton distance. The empty squares (and right ordinate) show the corresponding propagation delay along the 600 μm long axon, schematically represented in inset of Fig. 8 A. The arrow in the right ordinate indicates the propagation delay induced by a 600 μm long, 0.4 μm uniform axon.

Fig. 8 shows that for most realistic cases, in which the interbouton distance was found to range between 4–8 μm, the propagation velocity is lower than the velocity in a uniformly thin axon. Only when the interbouton distance is very small relative to the length of the bouton (and most of the axon consists of the large diameter), the propagation velocity is larger than the velocity in the thin axon. The conclusion is that, as a consequence of the frequent varicosities typically found along many axonal terminals, AP propagation within this region is slowed, and consequently the total delay is larger, compared with a homogeneous axon. Along the simulated axon, the delay contributed by the boutons can be calculated as the difference between the points labeled by the empty squares and the value corresponding to the arrow on the right ordinate. For example, with an interbouton distance of 4 μm this delay is ~0.3 ms (~15% of the total delay).[3]

Propagation delay in an anatomically characterized axonal tree

In this section, AXONTREE was used for estimating the propagation delays in an anatomically characterized

[3]In these simulations, the vertical walls of the boutons were neglected. Thus, for the interbouton and bouton diameters used in Fig. 8, the surface membrane area of the boutons was underestimated by a factor of 1.47. When the surface area of the vertical walls was incorporated in the model (by increasing both the membrane capacitance and conductance of each bouton by this factor; see Segev et al., 1991), the propagation velocity along the varicose region was found to be a few percents lower than shown in Fig. 8 B.

axon. In particular, we were interested in exploring the possibility that, within a single axon, the different synaptic outputs are activated asynchronously. For the simulation, a Horse Radish Peroxidase (HRP) labeled axon from the somatosensory cortex of the cat was digitized from Fig. 5 B of Schwark and Jones, 1989. This axon emerges from cortical layer V and projects mainly to area 4, but also sends collaterals to areas 3a and 3b (Fig. 9 A, scale bar = 300 μm). The terminal branches are studded with boutons (not shown). No details about diameters and about the presence of myelin were available. For the simulation, we have assumed that the diameter of the main process is 2.5 μm, the diameters of the first-order collaterals are 1 μm, whereas higher order collaterals have a diameter of 0.4 μm. All branches were assumed to be unmyelinated. Boutons were distributed every 4 μm along collaterals of second and higher order (a total of 977 boutons). Each bouton was modeled as a cylinder with a diameter and a length of 1.6 μm. These numbers are within the range reported by Schüz and Münster, 1985; Florence and Casagrande, 1987; Kisvarday et al., 1987; Peters, 1987; Rockland, 1989; Smith and Armstrong, 1990).

Frames B–D in Fig. 9 show the distribution of voltage (coded in *colors*) along the simulated axon at three different times (*upper left corner* of each frame). The current stimulus was injected to the leftmost compartment at time 0. It can be seen that the total propagation latency within this axon reaches several milliseconds. A significant (few milliseconds) difference in activation time of the proximal versus the distal boutons is also observed (compare Fig. 9 C with D). The latter point is emphasized in Fig. 10 A, where the distribution of AP peak time at the boutons of the simulated axon was calculated. Two populations are distinct in this histogram, one ranging from t_{peak} = 2.6 to 4.6 ms (3.8 ± 0.5 ms) and the other from t_{peak} = 4.6 to 6.6 ms (5.8 ± 0.4 ms). The first peak is contributed by terminals innervating areas 3a, 3b, and the proximal part of area 4. The second peak is contributed mainly by terminals innervating the distal part of area 4. The distribution of the anatomical distance of the boutons is shown in Fig. 10 B. Again, two populations are prominent. Note, however, that the shapes of the histograms in Fig. 10 A and B are different. This indicates that the distance of the boutons cannot, by itself, explain the distribution of AP peak times along the axon. In addition to the length of the axonal processes, the detailed geometry of the tree, including diameter changes, also contributes to the propagation delays along the axonal tree (see Discussion).
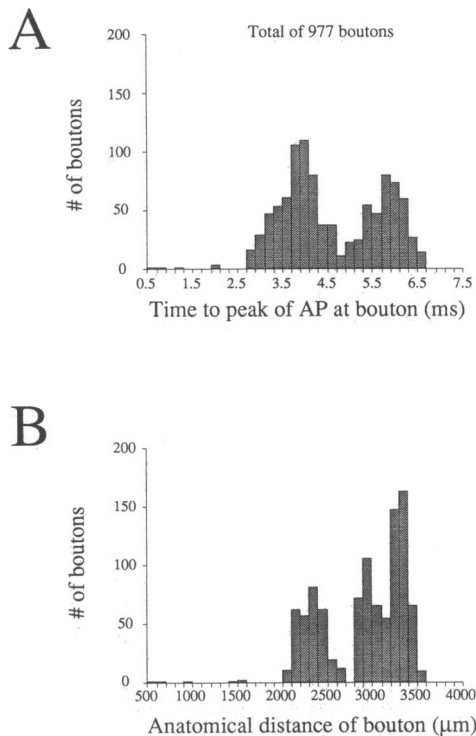
FIGURE 10 Asynchronous activation of the different release sites (axonal boutons) within a single axon. In *A*, the distribution of AP peak times at the different boutons of the axon simulated in Fig. 9 is shown. The distribution of the anatomical distances of these boutons is depicted in *B*. The first peak in *B* corresponds to boutons innervating cortical areas 3a and 3b and the proximal area of area 4, whereas the second peak corresponds to boutons innervating cortical distal area 4. See text for more details.

DISCUSSION

Recent advances in staining techniques, most notably the use of intracellular HRP injection, have brought a wealth of information regarding the fine structure of axons. Detailed measurements at light microscopic (LM) level have revealed the morphological complexity of axons; EM investigation allows identification of the exact sites (and types) of synapses that axons make with their targets (e.g., Gilbert and Wiesel, 1979; Schüz and Münster, 1985; Sereno and Ulinski, 1987). We now know that axons tend to ramify extensively and create frequent synaptic boutons (varicosities) along their terminals and collaterals. These boutons (the output sites of the axon) have a diameter which may be two to five times larger than that of the axon along the interbouton distance (e.g., Florence and Ca~agrande, 1987; Gerfen et al., 1987; Jensen and Killackey, 1987; Peters, 1987). What is the significance of the axonal branching geome-

try for the transmission and processing of the APs traveling along these axons?

To explore this and related functional questions, theoretical tools should be developed in parallel with the anatomical techniques mentioned above. These tools should allow one to focus on the interplay between axons morphology and their electrical function. As elaborated in the companion paper, AXONTREE is a simulator constructed specifically for this purpose. Here, it was used for two, somewhat different, but yet related, purposes. The first is to gain insights into the effect of isolated geometrical changes on the conduction velocity (delay) of the AP; our investigation focuses initially on a single change and then on two or more, electrically close, changes. Through this theoretical exploration several general rules could be formulated. The second purpose is to estimate the propagation delays to the different output sites of a reconstructed axon. We modeled a cortical axon from cat somatosensory cortex that was characterized at the LM level. Data on length and branching pattern was obtained from the LM study, whereas diameters and boutons distribution were estimated from other studies on cortical axons performed at the EM level. The main results are summarized below and their functional implications are considered.

Propagation delay at a single geometrical change

Fig. 3 shows that just before propagation failure, the delay (δt) that results from a single geometrical change in which the geometrical ratio increases (i.e., $GR > 1$), corresponding to a relative increase in diameter, may reach 1 ms for the Hodgkin and Huxley (1952) AP at 20°C. At 6.3°C, the delay may reach 2.3 ms and at 30°C it may reach only 0.3 mS. Hence, this delay depends strongly on the kinetics and the density of the excitable channels (currents) that carry the AP (Fig. 4). Clearly, the delay also depends on the passive properties of the axon. For example, the critical value of GR in which propagation fails depends on the value of g_L (the specific leak conductance). When g_L is increased from 0.3 to 1 ms/cm^2 and all other parameters are preserved as in Fig. 3, the critical GR is decreased from 10.5 to 8 and the maximal delay is now 0.85 ms (rather than 1 ms). This study did not focus on the dependence of δt on the different parameters, rather, it aimed at deriving general qualitative rules that do not depend on a particular set of parameters chosen.

Fig. 3 also demonstrates that δt is a supralinear function of GR when $GR > 1$. Hence, increasing a given $GR > 1$ by α would increase the propagation delay at that region by more than α (Fig. 3). Fig. 3 also shows that

for a given $GR > 1$, the delay is always larger than the speedup obtained at the reciprocal of that GR value. Thus, two successive geometrical irregularities, one with $GR > 1$ and the other with the reciprocal of that GR value, will produce a net positive delay (as compared with the homogeneous case). This is an important result because it implies that for an axon with a number of geometrical changes with $GR > 1$ and an identical number of changes with the inverse ratio, i.e., $1/GR$ such as the varicose axon illustrated in Fig. 8, the conduction velocity is lower than expected in a uniform axon whose diameter is the average between its thin and its thick parts.

Propagation delay and the interaction between successive geometrical changes

Our study shows that the delay that results from two successive, electrically adjacent geometrical changes, each with $GR > 1$ is larger than the linear sum of the two individual delays (Figs. 5 and 6). When both $GR < 1$, the speedup is less than that expected from the linear sum of the two.

The most interesting case occurs when an axon first becomes thicker (with $GR > 1$) and, some distance later, returns to its original diameter (i.e., $GR_2 = 1/GR_1$). As discussed above, the delay due to this kind of geometrical irregularity is always positive. Thus, such varicosities can act as a neuronal delay element. The total amount of the additional delay due to the two associated geometrical irregularities is small, usually less than 50 μs for realistic geometrical values. If, however, enough of these varicosities are located one after the other on an axon, like beads on a string, the total delay incurred by such a structure can exceed the delay associated with the axon without any varicosities (Fig. 8). Nonetheless, even here, the difference between a 600 μm long, thick axon without varicosities and the same axon with varicosities is less than a third of a millisecond (Fig. 8). One should note, however, that if the axonal terminals are endowed with slower channel kinetics or with a low density of excitable channels, the delay resulting from the presence of frequent varicosities may be significantly larger.

Delays in a reconstructed axonal tree

We also investigated the total delay and temporal dispersion expected in an anatomically characterized axonal tree in the last part of our study. We used a HRP-injected axon of an extensively braching, putative pyramidal cell from cat somatosensory cortex (Schwark and Jones, 1989, Fig. 5 B). Because no detailed EM data

characterizing the diameter and the myelinization are available for this axon, we used typical values derived from a number of other cortical cells. We assumed that the axon is unmyelinated, because most of it is confined to the grey matter. Moreover, no myelin appears to exist around varicosities and around thin branches in the terminal parts of the tree. Because the presence of myelin and the associated clustering of sodium channels in the nodal regions (Waxman and Ritchie, 1985) will speed up the propagation of APs, our model thus puts an upper bound on the delays expected in this axonal tree. Over the 3.5 mm extent of the tree, the total delay, measured from the injection point to the most distal bouton is 6.5 ms. The delay times fell into two groups, one corresponding to terminals innervating areas 3a, 3b and the proximal part of area 4, and the other corresponding to terminals innervating the distal part of area 4 (Fig. 9A). Within each group, the mean and the standard deviation was 3.8 ± 0.5 ms for the proximal group and 5.8 ± 0.4 ms for the distal group. Only ~0.4 ms for the distal group and 0.2 ms for the proximal group, i.e., ~6–7% of the mean is attributable to the presence of the varicosities. The effect of the branch points on the delay was much more significant; 1.49 ms for the distal group and 0.58 ms for the proximal group, i.e., 16–26% of the mean delay results from the presence of branch points. In other words, the pure delays from the axonal cables (placing the branches end to end and neglecting the intervening branch points and varicosities) account for most (67–78%) of the delay.

Functional consequences

It is interesting to consider whether the results presented in this paper have any possible functional consequences for the computations underlying neuronal information processing (Koch and Poggio, 1987). We will briefly consider the temporal dispersion and the total delay associated with axonal trees.

In principle, whether differences in synaptic activation time of the target cells are significant depends on the membrane time constant (τ_m) which governs the dynamics of the post-synaptic cell. For cells with a long membrane time constant (15–50 ms) as found in experimental conditions in cerebellar Purkinje cells (Segev et al., 1991) and pyramidal and stellate cortical cells (Douglas et al., 1991), a delay of a few milliseconds between inputs to the postsynaptic cell will be masked. If indeed such long time constants are the properties of cortical cells in the behaving animal (where background activity of many synapses may significantly reduce the effective τ_m), it appears that temporal dispersion of AP propagation in axonal trees has little (if any) functional consequences. Nevertheless, recent studies do suggest

that an important parameter for information processing in cortical networks is the timing of inputs converging on a single neuron (as, for instance, in the "synfire" model of Abeles, 1991). According to this model, a single cortical cell acts as a coincidence detector in the millisecond range. Here, axonal delays could play an important functional role.

Whether the propagation delay along axons is used in cortical computations is not yet clear. Yet, in some systems, the conduction delays along axons clearly have a functional significance. In the barn owl, for example, precise sound localization in the horizontal plane is achieved by measuring interaural time differences in the range of a tenth of a millisecond. This extraordinary temporal resolution is apparently based on small differences in conduction delays along afferents innervating the nucleus laminaris (Carr and Konishi, 1988). Furthermore, intracellular recordings from these afferents show orderly changes in conduction delay with depth in the nucleus. In this case, morphological irregularities may contribute to that delay function of the axon.

On the other hand, a number of neuronal operations, such as direction selectivity, seem to require a delay on the order of 20–30 ms (Koch et al., 1986). Given our range of parameters considered, only a small fraction of this delay could originate in the axonal tree for any computation which is performed locally, i.e., within a hypercolumn or two. It appears likely that such large delays are governed by two additional sources of delays in a single neuron. Namely, the delay imposed by the synaptic processes (the dynamics of neurotransmitters release and kinetics of the postsynaptic channels) and the delay contributed by the propagation of the synaptic potential along the dendritic tree. It is reasonable to conclude that different sources of delays within the single neuron (i.e., the axonal, the synaptic, and the dendritic) are used to perform different neuronal computations.

REFERENCES

Abeles, M. 1991. Corticonics. Cambridge University Press, Cambridge. 280 pp.

Berkenblit, M. B., N. D. Vvedenskaya, L. S. Gnedenko, S. A. Kovalev, A. V. Khopolov, S. V. Fomin, and L. M. Chaylakhyan. 1970. Computer investigation of the features of conduction of a nerve impulse along fibers with different degrees of widening. *Biofizika.* 15:1081–1089.

Carr, C. E., and M. Konishi. 1988. Axonal delay lines for time measurement in the owl's brainstem. *Proc. Natl. Acad. Sci. USA.* 85:8311–8315.

Douglas, R. J., K. A. C. Martin, and D. Whitteridge. 1991. An intracellular analysis of the visual responses of neurones in cat visual cortex. *J. Physiol. (Lond.).* 440:659–696.

Florence, S. L., and V. A. Casagrande. 1987. Organization of individual afferent axons in layer IV of striate cortex in a primate. *J. Neurosci.* 7:3850–3868.

Fyffe, R. E. W., and A. R. Light. 1984. The ultrastructure of group Ia afferent fiber synapses in the lumbosacral spinal cord of the cat. *Brain Res.* 300:201–209.

Gerfen, C. R., M. Herkenham, and J. Thibault. 1987. The Neostriatal mosaic:II. Patch- and Matrix-directed mesostriatal dopaminergic and non-dopaminergic systems. *J. Neurosci.* 7:3915–3934.

Gilbert, C. D., and T. T. Wiesel. 1979. Morphology and intracortical projections of functionally characterized neurones in the cat visual cortex. *Nature (Lond.).* 280:120–125.

Goldstein, S. S., and W. Rall. 1974. Changes in action potential shape and velocity for changing core conductor geometry. *Biophys. J.* 14:731–757.

Grossman, Y., I. Parnas, and M. E. Spira. 1979. Differential conduction block in branches of a bifurcating axon. *J. Physiol. (Lond.).* 205:283–305.

Hodgkin, A. L., and A. F. Huxley. 1952. A quantitative description of membrane current and its application to conduction and excitation in nerve. *J. Physiol. (Lond.).* 215:283–320.

Hsiao, C.-F., M. Watanabe, and Y. Fukuda. 1984. The relation between axon diameter and axonal conduction velocity of Y, X, and W cells in the cat retina. *Brain Res.* 309:357–361.

Huxley, A. F. 1959. Ion movements during nerve activity. *Ann. NY Acad. Sci.* 81:221.

Jack, J. J. B., D. Noble, and R. W. Tsien. 1975. Electrical Current Flow in Excitable Cells. Clarendon Press, Oxford. 518 pp.

Jensen, K. F., and H. P. Killackey. 1987. Terminal arbors of axons projecting to the somatosensory cortex of the adult rat. I. The normal morphology of specific thalamocortical afferents. *J. Neurosci.* 7:3529–3543.

Khodorov, B. I., and E. N. Timin. 1975. Nerve impulse propagation along nonuniform fibres (investigations using mathematical models). *Prog. Biophys. Mol. Biol.* 30:145–184.

Kisvarday, Z. F., K. A. C. Martin, M. J. Friedlander, and P. Somogyi. 1987. Evidence for interlaminar inhibitory circuits in the striate cortex of the cat. *J. Comp. Neurol.* 260:1–19.

Koch, C., T. Poggio, and V. Torre. 1986. Computations in the vertebrate retina: gain enhancement, differentiation and motion discrimination. *TINS* 9:204–210.

Koch, C., and T. Poggio. 1987. Biophysics of computation: neurons, synapses and membranes. *In* Synaptic Function. G. M. Edelman, W. E. Galland, and W. M. Cowan, editors. Neurosciences Institute. 637–698.

Lüscher, H.-R. and J. S. Shiner. 1990a. Computation of action potential propagation and presynaptic bouton activation in terminal arborizations of different geometries. *Biophys. J.* 58:1377–1388.

Lüscher, H.-R., and J. S. Shiner. 1990b. Simulation of action potential propagation in complex terminal arborizations. *Biophys. J.* 58:1389–1399.

Manor, Y., Y. Gonczarowski, and I. Segev. 1991. Propagation of action potentials along complex axonal trees: model and implementation. *Biophys. J.* Vol. 60.

Martin, K. A. C. 1984. Neuronal circuits in cat striate cortex. *In* Cerebral Cortex. Functional Properties of Cortical Cells. Vol. 2. E. G. Jones and A. Peters, editors.

McGuire, B. A., J. P. Hornung, C. D. Gilbert, and T. N. Wiesel. 1984. Patterns of synaptic input to layer 4 of the cat striate cortex. *J. Neurosci.* 4:3021–3033.

Moore, J. W., Stockbridge, N., and Westerfield, M. 1983. On the site of impulse generation in a neuron. *J. Physiol. (Lond.).* 336:301–311.

Ohgaki, T., I. S. Curthoys, and C. H. Markham. 1987. Anatomy of physiologically identified eye movement-related pause neurons in the cat: Pontomedullary region. *J. Comp. Neurol.* 266:56–72.

Paranas, I. 1972. Differential block at high frequency of branches of a single axon innervating two muscles. *J. Neurophysiol.* 35:903–914.

Parans, I., and I. Segev. 1979. A mathematical model for conduction of action potentials along bifurcating axons. *J. Physiol. (Lond.).* 295:323–343.

Peters, A. 1987. Synaptic specificity in the cerebral cortex. *In* Synaptic Function. G. M. Edelman, W. E. Galland, and W. M. Cowan, editors. Neurosciences Institute. 373–397.

Rockland, K. 1989. Bistratified distribution of terminal arbors of individual axons projecting from area V1 to middle temporal area (MT) in the macaque monkey. *Visual Neurosci.* 3:155–170.

Schüz, A., and Münster, A. 1985. Synaptic density on the axonal tree of a pyramidal cell in the cortex of the mouse. *Neuroscience.* 15:33–39.

Schwark, H. D., and E. G. Jones. 1989. The distribution of intrinsic cortical axons in area 3b of cat primary somatosensory cortex. *Expt. Brain Res.* 78:501–513.

Segev, I., M. Rapp, Y. Manor, and Y. Yarom. 1991. Analog and digital processing in single nerve cells: dendritic integration and axonal propagation. *In* Single Neuron Computation. T. McKenna, J. Davis, and S. F. Zornetzer, editors. Academic Press, Florida. In press.

Sereno, M. I., and P. S. Ulinski. 1987. Caudal topographic nucleus isthmi and the rostral nontopographic nucleus isthmi in the turtle, *Pseudemys scripta. J. Comp. Neurol.* 261:319–346.

Smith, D. O. 1983. Axon conduction failure under in vivo conditions in crayfish. *J. Physiol. (Lond.).* 344:327–333.

Smith, B. N., and W. E. Armstrong. 1990. Tuberal supraoptic neurons-I. Morphological and electrophysiological characteristics observed with intracellular recordings and biocytin filling *in vitro. Neuroscience.* 38:469–483.

Stone, J., and Y. Fukuda. 1974. Conduction velocity grouping in the cat's optic nerve classified according to their retinal origin. *Exp. Brain Res.* 13:489–497.

Waxman, S. G., and J. M. Ritchie. 1985. Organization of ion channels in the myelinated nerve fiber. *Science (Wash. DC).* 228:1502–1507.

Waxman, S. G., and W. M. L. Bennett. 1972. Conduction velocities of small myelinated and non-myelinated fibers in CNS. *Nature (Lond.).* 238:217–219.

Westerfield, M., R. W. Joyner, and J. M. Moore. 1978. Temperature sensitive conduction failure at axon branch points. *J. Neurophysiol.* 41:1–8.